Butterfly proboscis-inspired tight rolling tapered soft actuators

Chemical Communications

COMMUNICATION

Butterfly proboscis-inspired tight rolling tapered soft actuator

Jeroen A. H. P. Sol[a], Akhil R. Pekeeti[b], Nihit Vyas[b], Albertus P. H. J. Schenning[a,c], Ratna K. Annabattula[b,*], Michael G. Debije[a,*]

Received 00th January 20xx,
Accepted 00th January 20xx

DOI: 10.1039/x0xx00000x

www.rsc.org/

Liquid crystalline networks have been fashioned into thin films with tapered thicknesses, revealing the possibility of rolling up extremely tightly when triggered thermally or with light. Compared to the often limited bending shown previously in liquid crystal network actuators, these tapered films curl up several hundreds of degrees. Finite element results of simulated functionally graded thin films with tapered thickness corroborate well with experimental work.

The world of robotics is at a point of revolution—soft robots are poised to challenge for supremacy. In particular, in the fields of sustainable energy harvesting,[1] personal comfort[2] and biomedical engineering,[3] these remotely-addressable yet compliant materials are making great strides towards becoming the constituents of choice for many smart devices to come. For soft robotics researchers, the natural world is a great source of inspiration.[4–8] Nature provides insights for many of the solutions to engineering problems facing soft robotics today: microrobots based on bacteria[9] and electrospun water strider legs,[10] are two examples of using natural blueprints to generate novel man-made devices.

One of the prime candidate materials for bio-inspired soft robots are liquid crystal networks (LCNs), which are densely crosslinked polymers built up of reactive self-assembling monomers ("reactive mesogens").[11,12] The significance of LCNs in these developments are largely based on their anisotropic thermomechanical behaviour—upon disordering, LCNs shrink along the molecular director **n**, while perpendicular to **n** they expand.[13] LCNs have been used to create biomimetic soft actuators: caterpillar-like inching robots,[6] Venus flytrap-inspired grippers,[5] a high-power seedpod actuator,[7] or inspired by the locomotion of micro-organisms, "microrobots".[14,15]

Remarkably, all LCN-based actuators reported to date feature a uniform film thickness. Recently, a tapered paper-polyester bilayer was reported in which the tapered structure showed neat rolling and could be used to grapple objects.[16] However, in this case, the polyester acted as a shape memory material, meaning that autonomous actuation can only be performed once—in contrast to actuators based on LCNs, which are known to exhibit reversible motion.[13]

Previously shown splay-LCNs of constant film thickness typically bend up to a full rotation at elevated temperatures.[13] In this work, LCNs are made with a thickness taper along the length of the film, similar to the proboscis of butterflies, their feeding organ (see Figure 1a for a comparison).[17,18] At rest, it is coiled up under its head, taking up minimal space. In action, it can extend to the body length of the butterfly, and is used to retrieve nectar from plants, or nutrients from rotting fruits, depending on the species of butterfly.[19] Our proboscis-inspired tapered actuators show tight bending behaviour not seen in splay-LCNs before, with up to 3½ rotations upon heating or exposure to light. This rolling is fully reversible to reveal a nearly straight polymer strip at room temperature. Finite element modelling (FEM) results correspond well with experimental results. This allows for reversing the roles in the future, where the finite element model can be harnessed to anticipate the response of yet unexplored LC alignments and film geometries. Eventually, this could find use in designing LCN actuators that perform complex functions in larger soft robotic assemblies, or possibly as stand-alone devices in mixing systems for microfluidics.

The tapered-thickness, splay-aligned LCN thin films are obtained by filling alignment cells with a liquid crystal mixture consisting of equal weight fractions of monoacrylate **1** and diacrylate crosslinker **2** (see Figure 1d for structures, more experimental details in the Electronic Supporting Information, ESI). Photo-activated actuation is achieved through the

[a] Laboratory of Stimuli-responsive Functional Materials and Devices (SFD), Department of Chemical Engineering and Chemistry, Eindhoven University of Technology (TU/e), 5600 MB Eindhoven, The Netherlands, e-mail: m.g.debije@tue.nl
[b] Stimuli-Responsive Systems Laboratory, Department of Mechanical Engineering, Indian Institute of Technology Madras (IITM), 600036 Chennai, India, e-mail: ratna@iitm.ac.in
[c] Institute for Complex Molecular Systems (ICMS), Eindhoven University of Technology (TU/e), 5600 MB Eindhoven, The Netherlands.
Electronic Supplementary Information (ESI) available: [details of any supplementary information available should be included here]. See DOI: 10.1039/x0xx00000x

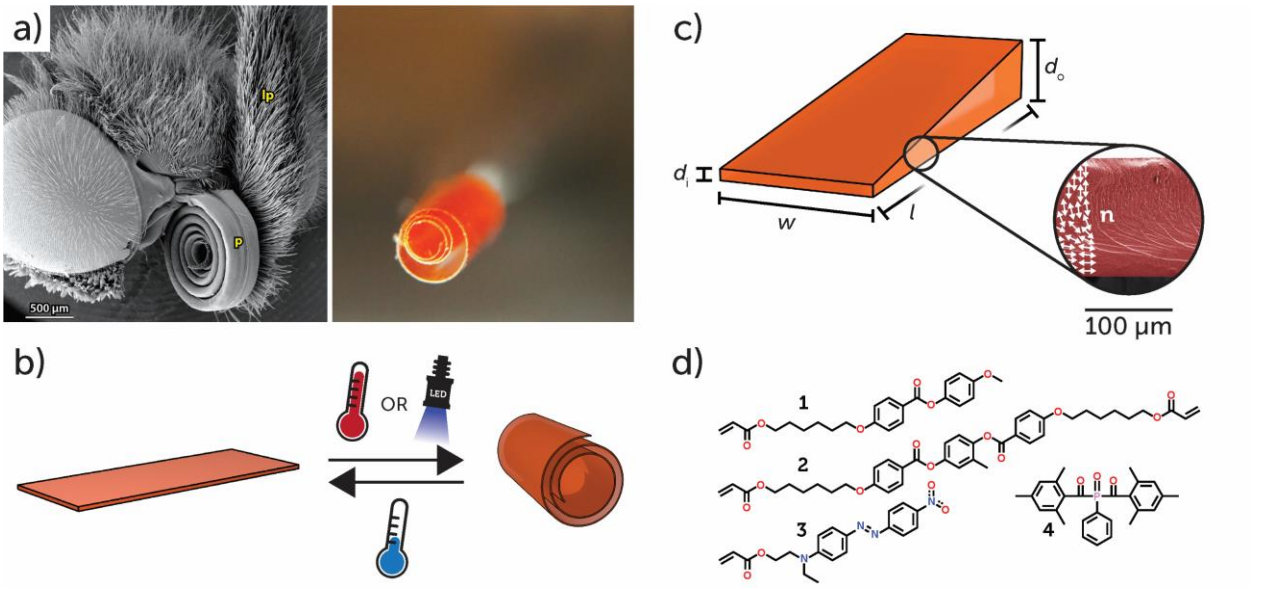

Figure 1. a) Head of a *Vanessa cardui* butterfly featuring its proboscis (p) in the resting position. Photograph reproduced from Krenn[19] with permission from *Annual Reviews Inc.* (right) A tightly rolled LCN film as described in this paper. b) Schematic of the tapered actuator film concept; upon temperature increase or by irradiating with 455 nm light, the splay LCN rolls into a proboscis-like shape. When the light source is removed or the temperature is decreased, the sample unrolls. c) Schematic showing the shape of a tapered LCN, depicting the molecular alignment **n** and other film characteristics such as aspect ratio l/w and thicknesses d_i and d_o Inset: cross-section of high-thickness splay-aligned LCN, featuring the molecular director (white arrows) as function of film depth. d) Reactive mesogens **1**-**3** and photo-initiator **4** used to fabricate the liquid crystalline network actuator.

incorporation of azobenzene dye **3**, which covalently bonds to the LCN during photo-polymerisation. Photoinitiation of the free radical polymerisation is accomplished by **4**. The phase behaviour of the mixture was studied by differential scanning calorimetry (DSC) and polarised optical microscopy (POM). These results indicate a transition from isotropic to nematic at 77 °C ($T_{N\text{-}I}$) when cooling, see Figure S2 for details.

Splay-aligned LC cells were made by sticking together glass with homeotropic and rubbed planar polyimide alignment layers facing each other. Spacer glue (10 µm) and double-sided tape (50 µm) was used to provide an LC alignment cell with tapered cell gap. These cells were filled with the LC mixture at 90 °C, above $T_{N\text{-}I}$. After filling, the temperature was lowered to 55 °C, whereupon the LCs self-assembled into the nematic mesophase. After photo-polymerisation to lock in the monomer's alignment, a thermal post-curing ensured maximum conversion of the acrylate groups (see Figure S3 for FT-IR data on C=C conversion). DSC reveals that the phase transition peak at $T_{N\text{-}I}$ has disappeared after polymerisation, as expected (see Figure S2). Cells were opened using a razor blade, revealing a thin film stuck to the glass coated with planar-aligned polyimide. Surface profilometry determined that film thicknesses were close to the spacer diameters chosen during cell manufacture. Furthermore, the thickness gradient between the thin and thick sides was linear. A polarised optical micrograph verified that the uniaxial nematic alignment was fixed during polymerisation, and dynamic mechanical analysis (DMA) revealed that the LCN has a broad glass transition range with the peak of tan(δ) at around 65 °C (T_g, see Figure S4). Scanning electron micrographs confirm that even at film thicknesses exceeding 100 µm, splay alignment is retained (see Figure 1c). The estimated ratios of penetration depth between homeotropic- and planar-aligned mesogens through the depth of the film depend on the film thickness (see Figure S5).

Films were cut from the LCN as a strip with a $\Delta d = (d_o - d_i) = 20$ µm, $d_{avg} = 25$ µm, $l/w = 4$ and the thickness taper Δd in the same direction as the nematic director **n** (see Figure 1c for a schematic image detailing these parameters). Upon removal of this film from the glass substrate, a free-standing film is obtained that shows no to little pre-bend, in which case the film slightly bends with the homeotropic side inward. This can be explained by the lower polymerisation temperature, which pre-empts the build-up of large thermal strains during polymerisation, and the thermal annealing, which also alleviates thermal stresses.[20]

The free-standing films were actuated in an oven with a window, through which photographs were recorded at set intervals. A digital temperature sensor recorded the temperature inside the oven at the same intervals. As the temperature was increased to 100 °C, the film rolled up tightly, with a curvature of several hundreds of degrees. This is best visualised by a series of photographs, as in Figure 2 (see ESI Video 1 for a time-lapse video).

This behaviour can be explained with Timoshenko's model for bimetallic strips in mind, which correlates film thickness to radius of curvature (r_C) for a given differential thermal strain.[21] In splay-aligned films with planar anchoring on one face of the film and homeotropic on the other, curling is observed typically up to a full rotation at elevated temperatures.[13] Later, the use of (reactive) azobenzene-containing dopants allowed for the LCN to be addressed and actuated with light.[1,5,6,22–28] Thus, the film shows an increasingly smaller r_C as the material becomes thinner, allowing it to effectively roll into itself.

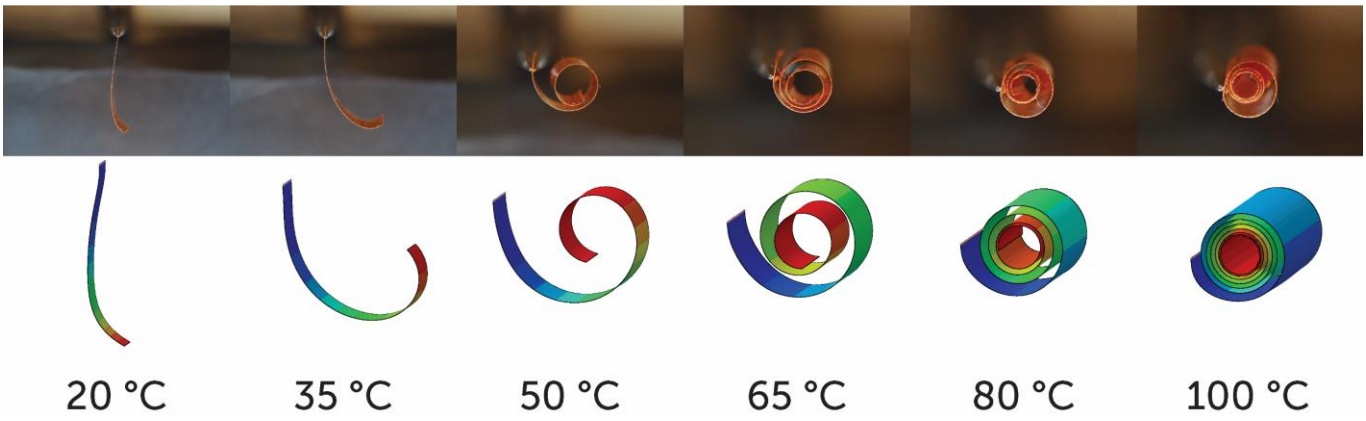

Figure 2. Comparison of experimental thermomechanical bending results (top) with finite element method results (bottom) for a tapered splay-aligned LCN film at different temperatures. Coloured regions in the finite element results correspond to film sections with equal r_C.

In order to better understand the bending behaviour of these tapered thickness LCNs, finite element simulations were performed. As described in more detail in the ESI, the tapered geometry along the length of the film is discretised using four-noded shell elements with composite sectional properties for the finite element model. The properties of the elastic moduli and the thermal expansion as a function of temperature were measured and used as input for the model (see Figure S4 and S6). The finite element model incorporates the variation of LC alignment direction through the depth of the film, thus making it a functionally graded system. The film is modelled as a three-layered system, in which each layer represents an area of the film with either homeotropic, planar or intermediate (45° tilt) alignments. The relative thickness of the layers is programmed according to the depths found with scanning electron microscopy (SEM), as seen in Figure S5. A video of the simulated functionally graded layer (ESI Video 2) shows that upon temperature increase, tight rolling takes place.

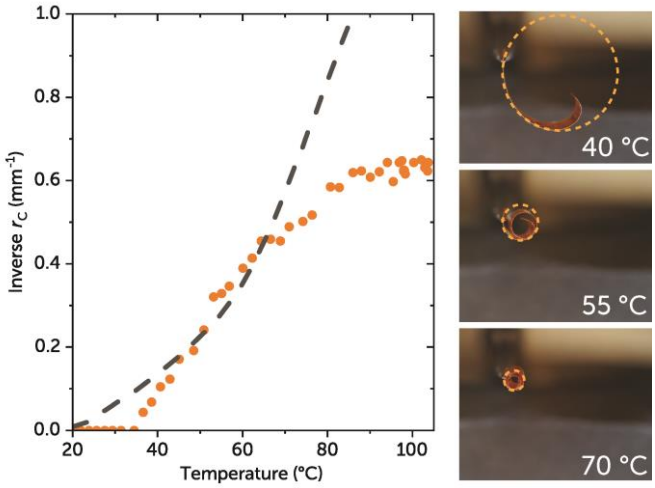

Figure 3. Plot showing measured r_C for the LCN film from Figure 2 at different temperatures (orange circles). The dashed grey line is composed of r_C values from finite element analysis. Photographs on the right side detail the measurement method for r_C.

There is good correspondence between the predicted shapes and those achieved in practice (see Figure 2), although the model somewhat overpredicts the bending behaviour of the film above 65 °C, the glass transition temperature. When plotting the inverse of the measured r_C (Figure 3), juxtaposed with the finite element result for r_C, the same trend is seen even more clearly. We postulate that this is a result of a few factors. Firstly, the elastic moduli (E' and E'') of the material diminish strongly above T_g, dropping at least an order or magnitude. However, as predicted by the model, the main driver for rolling is the ratio between elastic modulus parallel (E_{11}) and perpendicular ($E_{22,33}$) to **n**. From DMA results (Figure S4) it is seen that the ratio between these is not significantly influenced by the glass transition. On the contrary, self-contact by the film might lead to friction that hampers tighter rolling. This is especially relevant as the material has its T_g around 65 °C, above which it is soft, which could promote surface adhesion. We postulate that above T_g, a combination of this surface adhesion phenomenon, coupled with the lower absolute values of the elastic moduli is responsible for the model overpredicting.

So far, modelling results have pointed out that the number of rotations made during thermal actuation depend mainly on the difference between thermal expansion coefficients ($\Delta\alpha$) parallel and perpendicular to **n** (see Figure S6 for data on thermal strain).

To study the light response of the azobenzene-based LC material (compound **3**, "disperse red 1 acrylate"), it was irradiated with blue light (λ = 455 nm), activating the *trans-cis* isomerisation. As demonstrated in Figure S7bc, illumination from a single direction results in significant self-shading that prevents the film from bending fully into a rolled conformation. Turning on both light sources at once (Figure 4) allows for otherwise shaded azobenzene molecules to be addressed, resulting in formation of the anticipated tight curl. After turning off the light source, the film swiftly unbends, but with a

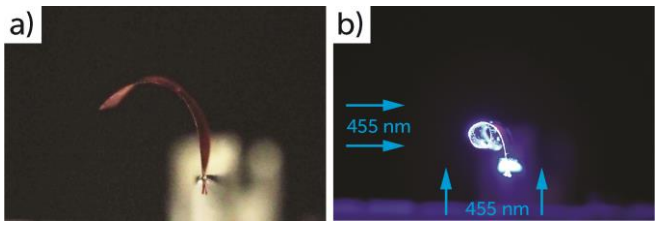

Figure 4. Tapered splay-aligned film irradiated with 455 nm light. a) No illumination, b) illumination from left and underneath at a total intensity of about 620 mW cm^{-2}, c) remaining "post-bend" after photo-actuation.

remaining "post-bend" (ESI Video 3) – we propose that this is due to vitrification during the backward motion, as actuation of the film happens around the material's T_g.

In summary, we have generated a series of LCN films from liquid crystalline networks that boast a tapered geometry, with one side of the film thinner than the other. Actuation triggered by heat or light results in smooth transition from fully extended to extremely tightly rolled morphologies, which are completely reversible and reproducible. Generation of actuators using tapered LCN films could allow more dramatic and consistent motions, allowing their application in a much broader range of devices to come. Our successful predictive model allows a wide exploration of potential actuation mechanisms to identify promising candidates to be produced experimentally.

Conflicts of interest

There are no conflicts to declare.

Notes and references

The authors would like to express their gratitude towards Simon J. A. Houben (TU/e) for recording SEM pictures, and Marina Pilz da Cunha (TU/e) and Rob C. P. Verpaalen (TU/e) for results interpretation, discussion and DMA measurements. This research received funding from the Netherlands Organisation for Scientific Research (NWO) in the framework of the Innovation Fund Chemistry and from the Dutch Ministry of Economic Affairs in the framework of the PPP allowance.

1 A. H. Gelebart, D. J. Mulder, M. Varga, A. Konya, G. Vantomme, E. W. Meijer, R. L. B. Selinger and D. J. Broer, *Nature*, 2017, **546**, 632.
2 F. L. L. Visschers, M. Hendrikx, Y. Zhan and D. Liu, *Soft Matter*, 2018, **14**, 4898.
3 M. Cianchetti, C. Laschi, A. Menciassi and P. Dario, *Nat. Rev. Mater.*, 2018, **3**, 143.
4 C. L. van Oosten, C. W. M. Bastiaansen and D. J. Broer, *Nat. Mater.*, 2009, **8**, 677.
5 O. M. Wani, H. Zeng and A. Priimagi, *Nat. Commun.*, 2017, **8**, 15546.
6 H. Zeng, O. M. Wani, P. Wasylczyk and A. Priimagi, *Macromol. Rapid Commun.*, 2018, **39**, 1700224.
7 S. J. Aßhoff, F. Lancia, S. Iamsaard, B. Matt, T. Kudernac, S. P. Fletcher and N. Katsonis, *Angew. Chem. Int. Ed.*, 2017, **56**, 3261; *Angew. Chem.*, 2017, **129**, 3309.
8 T. J. Wallin, J. Pikul and R. F. Shepherd, *Nat. Rev. Mater.*, 2018, **3**, 84.
9 S. Palagi and P. Fischer, *Nat. Rev. Mater.*, 2018, **3**, 113.
10 F. Bai, J. Wu, G. Gong and L. Guo, *ACS Appl. Mater. Interfaces*, 2014, **6**, 16237.
11 H. Zeng, P. Wasylczyk, D. S. Wiersma and A. Priimagi, *Adv. Mater.*, 2018, **30**, 1703554.
12 M. Lahikainen, H. Zeng and A. Priimagi, *Nat. Commun.*, 2018, **9**, 4148.
13 G. N. Mol, K. D. Harris, C. W. M. Bastiaansen and D. J. Broer, *Adv. Funct. Mater.*, 2005, **15**, 1155.
14 H. Zeng, P. Wasylczyk, C. Parmeggiani, D. Martella, M. Burresi and D. S. Wiersma, *Adv. Mater.*, 2015, **27**, 3883.
15 D. S. Wiersma, S. Nocentini, C. Parmeggiani, D. Martella and D. Nuzhdin, in *Optical Trapping and Optical Micromanipulation XIV*, eds. K. Dholakia and G. C. Spalding, SPIE, 2017, p. 99.
16 W. Wang, C. Li, M. Cho and S.-H. Ahn, *ACS Appl. Mater. Interfaces*, 2018, **10**, 10419.
17 H. W. Krenn and N. Mühlberger, *Zool. Anz.*, 2002, **241**, 369.
18 H. W. Krenn and N. P. Kristensen, *Eur. J. Entomol.*, 2004, **101**, 565.
19 H. W. Krenn, *Annu. Rev. Entomol.*, 2010, **55**, 307.
20 R. C. P. Verpaalen, M. G. Debije, C. W. M. Bastiaansen, H. Halilović, T. A. P. Engels and A. P. H. J. Schenning, *J. Mater. Chem. A*, 2018, **6**, 17724.
21 S. Timoshenko, *J. Opt. Soc. Am.*, 1925, **11**, 233.
22 T. J. White, *J. Polym. Sci. Part B: Polym. Phys.*, 2018, **56**, 695.
23 M. Yamada, M. Kondo, J. Mamiya, Y. Yu, M. Kinoshita, C. J. Barrett and T. Ikeda, *Angew. Chem. Int. Ed.*, 2008, **47**, 4986; *Angew. Chem.*, 2008, **120**, 5064.
24 M. Hendrikx, B. Sırma, A. P. H. J. Schenning, D. Liu and D. J. Broer, *Adv. Mater. Interfaces*, 2018, **5**, 1800810.
25 H. P. C. van Kuringen, Z. J. W. A. Leijten, A. H. Gelebart, D. J. Mulder, G. Portale, D. J. Broer and A. P. H. J. Schenning, *Macromolecules*, 2015, **48**, 4073.
26 A. H. Gelebart, M. K. McBride, A. P. H. J. Schenning, C. N. Bowman and D. J. Broer, *Adv. Funct. Mater.*, 2016, **26**, 5322.
27 T. J. White, R. L. Bricker, L. V. Natarajan, N. V. Tabiryan, L. Green, Q. Li and T. J. Bunning, *Adv. Funct. Mater.*, 2009, **19**, 3484.
28 J. Lv, Y. Liu, J. Wei, E. Chen, L. Qin and Y. Yu, *Nature*, 2016, **537**, 179.